Transonic Computations About Complex Configurations Using Coupled Inner and Outer Flow Equations

Uno G. Nävert* and Yngve C-J. Sedin†
SAAB-SCANIA AB, Linköping, Sweden

Modern aircraft, particularly fighters, are characterized by a high degree of geometrical complexity. In transonic computations about such configurations, small disturbance (TSP) formulations on Cartesian grids offer a robust and cost-effective alternative to more elaborate methods in many engineering applications. Wing boundary conditions are then easily imposed using thin-wing theory, whereas fuselage boundary conditions usually are more difficult to implement. This paper presents a numerical method for solving the TSP equation about a complex slender configuration emphasizing a consistent treatment of the boundary conditions on the fuselage surface. The basic concept is a decomposition into two coupled inner and outer problems, using the theory of matched asymptotic expansions as guidance. The outer problem is discretized using a standard three-dimensional finite-difference scheme. The inner problem, enforcing the fuselage boundary conditions, is solved as a sequence of crossflow problems, using a linear two-dimensional panel method. Several test runs on a CRAY-1 computer have demonstrated the reliability and robustness of the above procedure. Computed pressure distributions for a number of three-dimensional cases, including one of the fighter type, are in good agreement with wind tunnel test data.

I. Introduction

In practical aerodynamic design and analysis work there is a wide scale of methodological needs, ranging from linear panel methods to more elaborate nonlinear techniques. Although in recent years great progress has been made in the Euler and Navier-Stokes methods,[6,8] they still are complicated and expensive to operate in three-dimensional everyday engineering work. In particular, they require an efficient and flexible grid generation process that still has to be invented to cover all of the different details of an aircraft in a rapid and efficient way.

Two decades ago, Woodward,[15] among others, developed a panel method that became a widespread tool in many aircraft industries. With this simple but flexible method, a large variety of aerodynamic problems could be tackled, including wing-body combinations, external stores, and static aeroelasticity.[5] The results gave qualitative and quantitative guidelines for many aerodynamic problems and opened up the use of computational aerodynamics in practice.

Recalling the rapid evolution of nonlinear computational methods during the 1970's,[7] it should be possible to develop a similar practical method as flexible and accessible as Woodward's, but now including nonlinear transonic flow. Steps in this direction were taken earlier, e.g., by Boppe.[4] The present paper has the same goal, but the approach is somewhat different.

One key feature to the success of the Woodward-type panel method was the simple treatment of the boundary conditions that were applied on mean surfaces or interference shells. This enabled rapid and flexible changes of the geometry without having to repanel the computed object. The background to this, of course, lies in the small disturbance assumption. Hence, using the same philosophy in nonlinear transonic flow, we are led to the transonic small perturbation (TSP) formulation that would give us a similar flexibility.

The present method utilizes the fact that in transonic flow the lateral interaction is very stiff and almost incompressible. Hence, an inner linear crossflow equation is combined with an outer nonlinear TSP equation using the theory of matched asymptotic expansions[2] as guidance. The inner and outer solutions are coupled along a rectangular, parallelepiped enclosing the aircraft fuselage. The boundary conditions on lifting surfaces are imposed on mean surfaces. Thus, a flexible method is found for complicated configurations using a simple Cartesian grid for the outer flow.

The method is capable of handling fighter-type configurations, including lifting surfaces, fuselage with canopy and air intake, and a vertical fin. External loads will be incorporated in the near future. Techniques using local grid refinements are also studied, and a convenient data structure for this is found.

Efforts to incorporate fuselage effects using a linear panel method were reported earlier.[14] However, the interactive transonic coupling of inner and outer flowfields was not considered.

II. Basic Concept: Coupled Inner and Outer Problems

We shall consider three-dimensional flow about a combination of a thin wing W, and a slender body mounted on a sting B at a small angle of attack α, relative to a subsonic freestream of velocity U_∞, and Mach number M_∞ close to unity. The configuration is symmetric with respect to the xz-plane of a Cartesian coordinate system (x,y,z), having its x axis aligned with the longitudinal axis of the body (see Fig. 1).

Assuming irrotational flow, we introduce the velocity potential Φ and the disturbance potential ϕ related by

$$\Phi = U_\infty[x\cos\alpha + z\sin\alpha + \phi] \tag{1}$$

Normalizing to $U_\infty = 1$ the local Mach number M for small disturbances is given by[10]

$$M^2 = M_\infty^2 + M_\infty^2[3 - (2-\gamma)M_\infty^2]\phi_x \tag{2}$$

Here $\gamma = 1.4$ is the specific heat ratio.

For an isolated wing of thickness ratio $\tau_w \ll 1$, thin wing theory gives[2]

$$T\phi \equiv (1-M^2)\phi_{xx} + \phi_{yy} + \phi_{zz} \simeq 0 \tag{3a}$$

Close to the wing this relation is simplified to

$$\phi_{zz} \simeq 0 \tag{3b}$$

Presented as Paper 86-1.3.4. at the 15th Congress of the International Council of Aeronautical Sciences, London, England, Sept. 7–12, 1986; received Sept. 9, 1986; revision received Oct. 26, 1987.

*Research Scientist, Computational Aerodynamics.
†Senior Research Scientist, Computational Aerodynamics.

(In our body-fixed coordinate system, a more elaborate expression for $T\phi$ contains α terms, $-2\alpha M_\infty^2\phi_{xz}$, and higher order terms. Since we assume α to be small, these terms are neglected. Numerical experiments incorporating the term $-2\alpha M_\infty^2\phi_{xz}$, indeed, give negligible differences in the test cases considered below.)

For an isolated body of thickness ratio $\tau_b \ll 1$, slender body theory gives

$$T\phi \simeq 0 \tag{4a}$$

or, close to the body,

$$L\phi \equiv \phi_{yy} + \phi_{zz} \simeq 0 \tag{4b}$$

Let us define an infinite parallelepiped P, with edges parallel to the x axis, encompassing the body and the innermost part of the wing. The interior and exterior of P outside W and B are denoted by P^i and P^e, respectively. Motivated by Eqs. (3) and (4), we now require the disturbance potential ϕ for the wing-body combination to satisfy

$$T\phi = 0 \quad \text{in } P^e \tag{5a}$$

$$L\phi = 0 \quad \text{in } P^i \tag{5b}$$

These outer and inner equations are coupled via compatibility conditions on the surface ∂P of P, where ϕ and its normal derivative ϕ_n are required to be continuous (see Fig. 2).

The longitudinal coupling for the inner problem is entirely provided by the boundary conditions set by the outer solution on ∂P. In case of a shock surface penetrating ∂P, the jump in ϕ_x admitted in the outer solution will thus have an impact also on the inner solution, although the potential is continuous across the shock.

To formulate boundary conditions for the wing, we write the equation satisfied by a point (x,y,z) on the wing surface ∂W as

$$z - Z(x,y) = 0 \quad \text{on } \partial W$$

where $Z(x,y)$ denotes one of the two functions $Z^-(x,y)$ and $Z^+(x,y)$, defining the lower and upper wing surfaces, respectively. The tangential flow boundary condition is then given by

$$\nabla\Phi \cdot (-Z_x, -Z_y, 1) = 0 \quad \text{on } \partial W$$

or, using Eq. (1) with $|\alpha| \ll 1$,

$$\phi_z = (1+\phi_x)Z_x + \phi_y Z_y - \alpha \quad \text{on } \partial W \tag{6}$$

As suggested by Eq. (3b), outside P this condition is imposed on a plane mean surface ∂W° at a constant $z = Z^\circ$, rather than on the physical wing surface ∂W. Equation (5a) is then extended to contain P°, defined as the exterior of P outside ∂W°. It is important to keep the term $(1+\phi_x)$ multiplying Z_x in Eq. (6).

The potential ϕ is continuous, except in points (x,y,Z°) on the wake downstream of ∂W°. Here, the Kutta condition admits potential jumps equal to the circulation $\Gamma(y)$, i.e., potential jumps that do not depend on x. The circulation distribution $\Gamma(y)$ is given by the difference in potential between the upper and lower wing surfaces at the trailing edge.

The tangential flow condition on the body surface ∂B is given by

$$\nabla\Phi \cdot (n_x, n_y, n_z) = 0 \quad \text{on } \partial B$$

where (n_x,n_y,n_z) is the outward unit normal on the body surface.

Expressing this as a condition for the crossflow velocity ϕ_n, given by

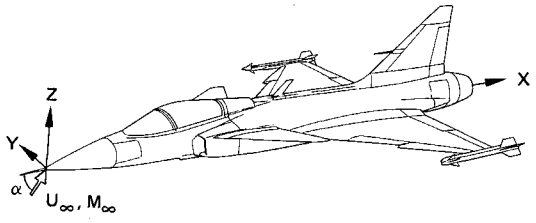

Fig. 1 Cartesian coordinate system.

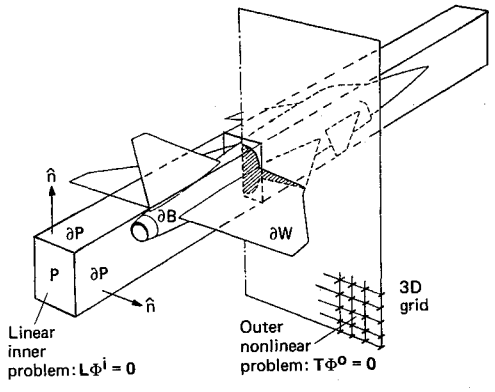

Fig. 2 Coupled inner and outer problems.

$$\phi_n \equiv (\phi_y, \phi_z)\cdot(n_y,n_z)/\sqrt{n_y^2+n_z^2} \quad \text{on } \partial B$$

we obtain, using Eq. (1) with $|a| \ll 1$ and $|\phi_x| \ll 1$,

$$\phi_n = h(x,y,z) \equiv (-n_x - \alpha n_z)/\sqrt{n_y^2+n_z^2} \quad \text{on } \partial B \tag{7}$$

This type of condition is also used on that part of the wing surface ∂W that is inside P.

In the far field, except for Trefftz's plane, we impose Dirichlet boundary conditions $\phi = g$, with g given by the expressions derived by Klunker[9] for a thin wing. In Trefftz's plane Π, given by

$$\Pi \equiv \{(x,y,z): x = \text{const} \to \infty\}$$

representing downstream infinity, we decompose ϕ as $\phi = \phi' + \phi''$. Here $\phi' = g$ is given by Klunker's expressions and ϕ'' represents the influence of the body. To determine ϕ'', we solve $L\phi'' = 0$ in Π, with the boundary condition $\phi_n'' = h - g_n$ [see Eq. (7)] imposed on the strong contour. The function g depends on the circulation Γ and has to be updated during the solution process.

III. Discretization

The outer and inner problems introduced in the previous section are restricted to finite computational domains $D^\circ \equiv P^\circ \cap D$ and $D^i \equiv P^i \cap D$, where D is defined by

$$D \equiv \{(x,y,z): x\min \le x \le x\max, 0 \le y \le y\max, z\min \le z \le z\max\}$$

The far-field boundary conditions are imposed on the boundary ∂D of D, as described in Sec. II.

We shall now in turn discuss discretization in D°, in D^i, and in Trefftz's plane Π at $x = x\max$. We denote the inner solution, i.e., the restriction of ϕ to D^i, by $\psi = \psi(x;y,z)$ to emphasize the two-dimensional character of the inner problem.

Discretization of the Outer Problem

The outer problem is given by

$$T\phi = (1-M^2)\phi_{xx} + \phi_{yy} + \phi_{zz} = 0 \quad \text{in } D^\circ \tag{8a}$$

$$\phi_z = (1+\phi_x)Z_x + \phi_y Z_y - \alpha \quad \text{on } \partial W^\circ \tag{8b}$$

$$\phi_n = \psi_n \quad \text{on } \partial P \cap D \tag{8c}$$

$$\phi = g \quad \text{on } \partial D \cap P^\circ \tag{8d}$$

The governing nonlinear operator T is of mixed type, being elliptic in subsonic regions ($M < 1$) and hyperbolic in supersonic regions ($M > 1$). The right-hand sides of the boundary conditions all depend on the solution and must be determined iteratively. This procedure is discussed in Sec. V.

Equation (8a) is discretized using Murman's type-dependent fully conservative scheme[11] on a Cartesian grid (see Fig. 3).

Below, we give the resulting difference equations for a uniform grid indexed by i,j,k, with grid size $\Delta x,\Delta y,\Delta z$, i.e., $\phi_{ijk} = \phi(i\Delta x, j\Delta y, k\Delta z)$. We use the convention that indices that are omitted have the value i, j, or k, i.e., $\phi_{i+1} = \phi_{i+1,jk}$, and so on. With

$$s_{ijk} \equiv 1 - M_\infty^2 - M_\infty^2[3 - (2-\gamma)M_\infty^2](\Delta x)^{-1}(\phi_{i+1} - \phi_{i-1})/2$$

$$\mu_{ijk} \equiv 0 \text{ if } s_{ijk} > 0 \quad \text{(subsonic flow)}$$

$$\mu_{ijk} \equiv 1 \text{ if } s_{ijk} < 0 \quad \text{(supersonic flow)}$$

$$p_{ijk} \equiv s_{ijk}(\Delta x)^{-2}(\phi_{i-1} - 2\phi_i + \phi_{i+1})$$

$$q_{ijk} \equiv (\Delta y)^{-2}(\phi_{j-1} - 2\phi_j + \phi_{j+1})$$

$$r_{ijk} \equiv (\Delta z)^{-2}(\phi_{k-1} - 2\phi_k + \phi_{k+1})$$

the difference approximation of Eq. (8a) reads

$$(1 - \mu_{ijk})p_{ijk} + \mu_{i-1,jk}p_{i-1,jk} + q_{ijk} + r_{ijk} = 0 \tag{9a}$$

We note that upstream differencing is used in the x direction in the case of supersonic flow. In shock points, we have $1 - \mu_{ijk} = \mu_{i-1,jk} = 1$ and in sonic points, $1 - \mu_{ijk} = \mu_{i-1,jk} = 0$.

Let (x_i,y_j,Z°) be a point on the wing mean surface ∂W°, which is placed halfway between two grid planes, indexed by K and $K+1$, for instance. The boundary condition in Eq. (8b) is imposed by defining

$$\begin{aligned} r_{ij,K} &\equiv (\Delta z)^{-1}\{\phi_z - (\Delta z)^{-1}(\phi_K - \phi_{K-1})\} \\ r_{ij,K+1} &\equiv (\Delta z)^{-1}\{(\Delta z)^{-1}(\phi_{K+1} - \phi_K) - \phi_z\} \end{aligned} \tag{9b}$$

with ϕ_z taken from Eq. (8b). The Kutta condition is implemented by defining

$$r_{ij,K} \equiv (\Delta z)^{-2}\{\phi_{K-1} - 2\phi_K + \phi_{K+1} - \Gamma\}$$

$$r_{ij,K+1} \equiv (\Delta z)^{-2}\{\phi_K + \Gamma - 2\phi_{K+1} + \phi_{K+2}\}$$

in points (x_i,y_j,Z°) on the wake.

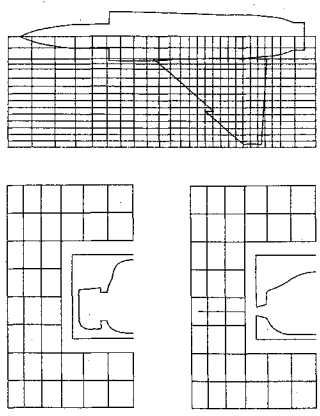

Fig. 3 Example of Cartesian computational grid.

Discretization of the Inner Problem

The inner problem is given by

$$L\psi = \psi_{yy} + \psi_{zz} = 0 \quad \text{in } D^i \tag{10a}$$

$$\psi_n = h \quad \text{on } (\partial B \cup \partial W) \cap D \tag{10b}$$

$$\psi = \phi \quad \text{on } \partial P \cap D \tag{10c}$$

This problem has an entirely different character from the outer problem [Eqs. (8)] since the governing operator L is linear and two-dimensional. For each grid plane P at $x = x_i$, we discretize [Eqs. (10)] in the intersection $D_i \equiv P_i \cap D^i$ using a panel method. The boundary

$$\partial D_i \equiv (\partial B \cup \partial W \cup \partial P) \cap D_i$$

of D_i is replaced by a family of straight panels, where each panel has a constant source distribution. Downstream of the wing we also introduce doublet panels along the wake contour $\partial W \cap D_i$ (see Fig. 4).

The doublet strengths are given by the potential jumps at the wing trailing edge. The source strengths are determined so that the boundary conditions are satisfied in the panel midpoints. For each D_i, we obtain a dense linear system of equations and the discrete problem can be written

$$A_i S_i = B_i, \qquad 1 \le i \le i\max \tag{11}$$

Here, $\{A_i\}$, $\{S_i\}$, and $\{B_i\}$ denote the system matrices, source strength vectors, and right-hand sides, respectively.

The inner flow equation (4b) is only valid to a distance $O(\tau_b)$ from the body in a subsonic case and to $O(1)$ in a transonic case.[2] So it is natural to place the parallelepiped surface ∂P at a distance $O(\tau_b)$ from the body centerline. At the same time, to avoid numerical difficulties in the panel method, we must have a certain minimum distance or gap between ∂P and the body surface. Both requirements have been found to be met by using horizontal and vertical gaps of 5% of the maximum body width and height, respectively.

The wing frequently requires a higher resolution power of the grid than is necessary (or even applicable, if the quality of the defining geometry is poor) for the body. In such cases it is sufficient to solve Eq. (11) for a subset of $\{i = 1 \ldots i\max\}$ and use a nonoscillatory interpolation procedure[1] to get normal derivatives on ∂P in intermediate planes as required in Eq. (8c).

Discretization in Trefftz's Plane

In Trefftz's plane Π, we solve the Laplacian problem

$$L\theta = \theta_{yy} + \theta_{zz} = 0 \quad \text{in } \Pi \backslash B \tag{12a}$$

$$\theta_n = h - g_n \quad \text{on } \partial B \cap \Pi \tag{12b}$$

where g and h were introduced in Sec. II. This problem is discretized and solved by a panel method, as described in the previous subsection. The disturbance potential ϕ in Π is then given by $\phi = \theta + g$.

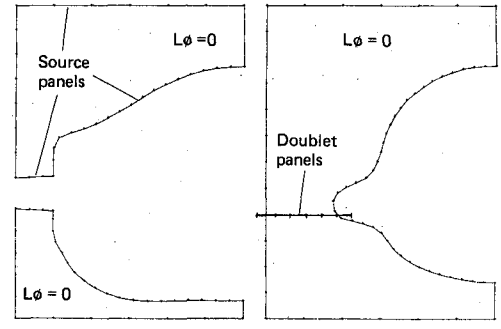

Fig. 4 Example of paneling of cross cuts containing wing or wake.

IV. Relaxation Procedure

The discrete outer problem [Eqs. (9)] is solved by successive line over-relaxations. In each iteration cycle, the grid is swept plane by plane in the x direction, and within each plane, line by line in the y direction, with only one line sweep in each plane per cycle.

Let ϕ and ϕ^+ denote the potentials before and after one iteration cycle. Further, define an intermediate potential ϕ' by

$$\phi' \equiv \omega^{-1}\phi^+ + (1-\omega^{-1})\phi$$

where ω is the over-relaxation factor, below chosen as 1.8. Then ϕ^+ is given by[3]

$$(1-\mu_{ijk})p'_{ijk} + \mu_{i-1,jk}p'_{i-1,jk} + q'_{ijk} + r'_{ijk} = 0 \qquad (13)$$

where in subsonic flow, i.e., $\mu_{ijk} = 0$

$$p'_{ijk} \equiv s_{ijk}(\Delta x)^{-2}(\phi^+_{i-1} - 2\phi'_i + \phi_{i+1})$$
$$q'_{ijk} \equiv (\Delta y)^{-2}(\phi^+_{j-1} - 2\phi'_j + \phi_{j+1})$$
$$r'_{ijk} \equiv (\Delta z)^{-2}(\phi^+_{k-1} - 2\phi^+_k + \phi^+_{k+1})$$

and in supersonic flow, i.e., $\mu_{ijk} = 1$

$$p'_{ijk} \equiv s_{ijk}(\Delta x)^{-2}(\phi_{i-1} - 2\phi^+_i + 2\phi_{i+1} - \phi_{i+1})$$
$$q'_{ijk} \equiv (\Delta y)^{-2}(\phi^+_{j-1} - \phi^+_j - \phi_j + \phi_{j+1})$$
$$r'_{ijk} \equiv (\Delta z)^{-2}(\phi^+_{k-1} - 2\phi^+_k + \phi^+_{k+1})$$

Introducing $c \equiv \phi^+ - \phi$, we finally rewrite Eq. (13) in correction form, ending up with a tridiagonal linear system

$$T_1 c_{k-1} + T_2 c_k + T_3 c_{k+1} = -R - t_1 c_{i-1} - t_2 c_{j-1} \qquad (14)$$

Here the residual R and the coefficients T_1, T_2, T_3, t_1, t_2 are given by

$$R \equiv (1-\mu_{ijk})p_{ijk} + \mu_{i-1,jk}p_{i-1,jk} + q_{ijk} + r_{ijk}$$
$$T_1 \equiv (\Delta z)^{-2}$$
$$T_2 \equiv -(\Delta x)^{-2}[2\omega^{-1}(1-\mu_i)s_i - 2\mu_{i-1}s_{i-1}]$$
$$-(\Delta y)^{-2}[2\omega^{-1}(1-\mu_i) + \mu_i] - 2(\Delta z)^{-2}$$
$$T_3 \equiv (\Delta z)^{-2}$$
$$t_1 \equiv (\Delta x)^{-2}[(1-\mu_i)s_i - 2\mu_{i-1}s_{i-1}]$$
$$t_2 \equiv (\Delta y)^{-2}$$

This discrete inner problem was formulated above as a sequence of dense linear systems

$$A_i S_i = B_i, \quad 1 \le i \le i\max \qquad (15)$$

[see Eq. (11)]. Due to the compatibility condition [Eq. (10c)], the vectors $\boldsymbol{B}_i$ are solution-dependent and must be determined in an iterative fashion. Since Eq. (15) thus has to be solved several times with different right-hand sides, we invert each A_i and save the inverse matrices on secondary storage. A special computation with the boundary condition [Eq. (10c)] omitted [and panels along the wing-body perimeter in Eq. (10b) only] is done to find an initial approximation ψ° to ψ.

V. Iterative Coupling Procedure

The coupling between the outer and inner problems is effected by the compatibility conditions (8c) and (10c). We may view the solving of Eq. (10) as a procedure for updating the boundary condition (8c). Rather than performing a large number of sweeps according to Eq. (14), with ψ_n fixed in Eq. (8c), we use the following strategy:

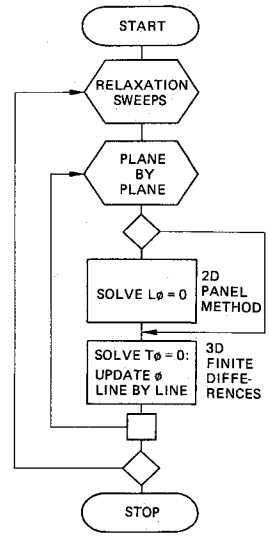

Fig. 5 Iteration process.

Step 1: Compute a start approximation ψ° as described above and solve Eq. (14) for ϕ^+ with $\phi = 0$.

Step 2: Perform a sequence of relaxation sweeps according to Eq. (14), with the normal derivative of ψ on the parallelepiped surface, ψ_n in the boundary condition (8c), updated by solving Eq. (15) for each sweep. Proceed until the maximum change in ψ_n from one sweep to the next has decreased by half a decade.

Step 3: Perform a sequence of relaxation sweeps according to Eq. (14), keeping ψ_n in Eq. (8c) fixed. Proceed until the maximum potential correction $c\max$ from one sweep to the next has decreased by half a decade.

Repeat steps 2 and 3 until some stopping criterion is satisfied, typically $c\max < 10^{-4}$.

Updating of the solution dependent boundary conditions (8b) and (8d) is done similarly with the test quantity in Step 2 replaced by "maximum change in ϕ on the wing surface" and "maximum change in circulation", respectively.

(The procedure described above is not a full matching of the inner and outer solutions, since second and higher order derivatives are not connected.)

A schematic picture of the iterative solution procedure is given in Fig. 5.

VI. Numerical Computations

We shall use the method described above to compute pressure distributions in transonic flow for three different configurations: an analytically defined bumpy and indented body,[12] the RAE wing-body combination,[13] and a wing-fuselage fighter configuration that has been wind tunnel tested by SAAB. The normalized pressure coefficient C_p is computed using the formula

$$C_p = -2\phi_x - (1-M_\infty^2)\phi_x^2 - \phi_y^2 - \phi_z^2$$

Computational Grids

For each configuration we use a sequence of nonuniform Cartesian computational grids of the type shown in Fig. 3.

The mean surface of the wing is placed halfway between two horizontal grid planes $z = z_K$ and $z = z_{k+1}$. Vertical grid planes cutting the wing have related spacings in the x and y directions so that at each span station $y = y_j$ the x coordinate of the leading edge is halfway between two grid planes $x = x_i$ and $x = x_{i+1}$. The y coordinate of the wing tip is halfway between

two grid planes $y = y_j$ and $y = y_{j+1}$. The step size Δz across the mean plane of the wing is typically 50% larger than the minimum step size Δx across the leading edge.

The resolution power of each grid is controlled by four parameters setting the relative resolution at the nose of the body, at the body-sting junction, at the wing root leading edge, and at the wing tip leading edge. For the RAE wing-body these parameters were 5, 5, 4, and 4%, resulting in 927,000 points for the finest grid. The corresponding data for the fighter configuration were 2, 5, 1, and 5%, and 3.4 million points. The results presented for the analytically defined body were obtained on a grid with 45,000 points.

Computed Pressure Distributions

Results for the analytically defined body are shown in Fig. 6. Computed pressures are in good agreement with wind tunnel data. We note that the positive peak in the computed C_p curve on the indented part of the surface is less pronounced in the wind tunnel data, probably because of viscous boundary-layer effects.

Figure 7 shows results for the RAE wing-body combination in a lifting case. We note that the suction peaks on the body surface induced by the presence of the wing are remarkably accurate. In the domain just upstream of the wing, the increase in pressure due to flow stagnation is underpredicted. Qualitatively, leaving out the ϕ_{xx} term in the inner problem will have this effect, as can be seen by applying Green's formula to the TSP equation [Eq. (5a)] inside the parallelepiped P.

The pressure distributions on the RAE wing are given at three different spanwise locations in Fig. 7. The agreement between computations and experiments is good and the shock is in its right position. At the wing tip, the suction peak is underpredicted due to an insufficient resolution power of the grid in this region. We also note a certain disagreement at the trailing edge close to the body.

Results for the fighter configuration are shown in Fig. 8. The fuselage geometry of this wind tunnel model contains some

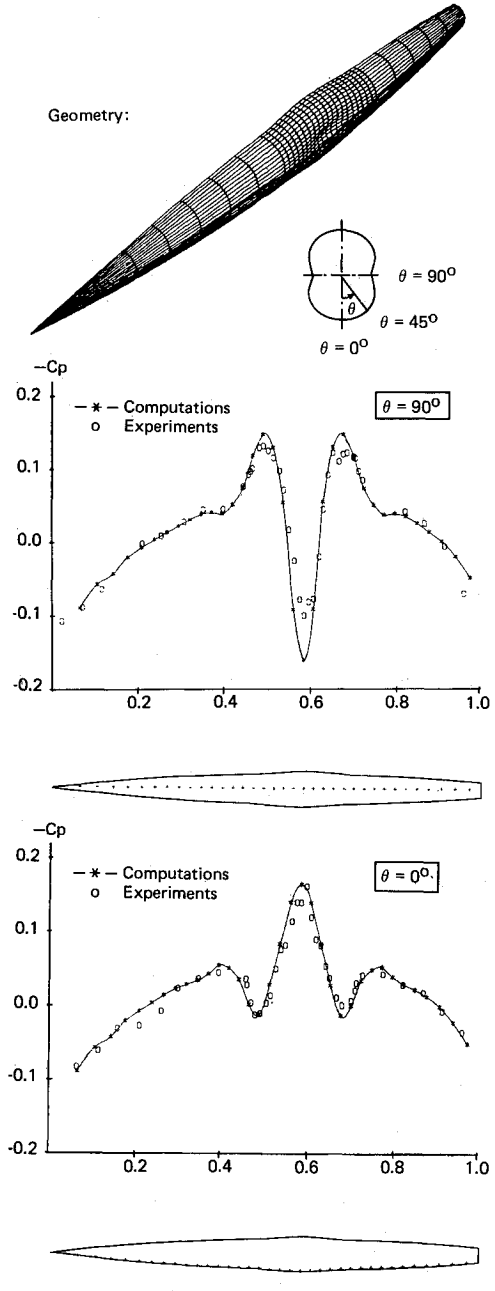

Fig. 6 Computed and experimental[12] pressure signatures for a bumpy and indented body at $M_\infty = 0.95$, $\alpha = 0$ deg.

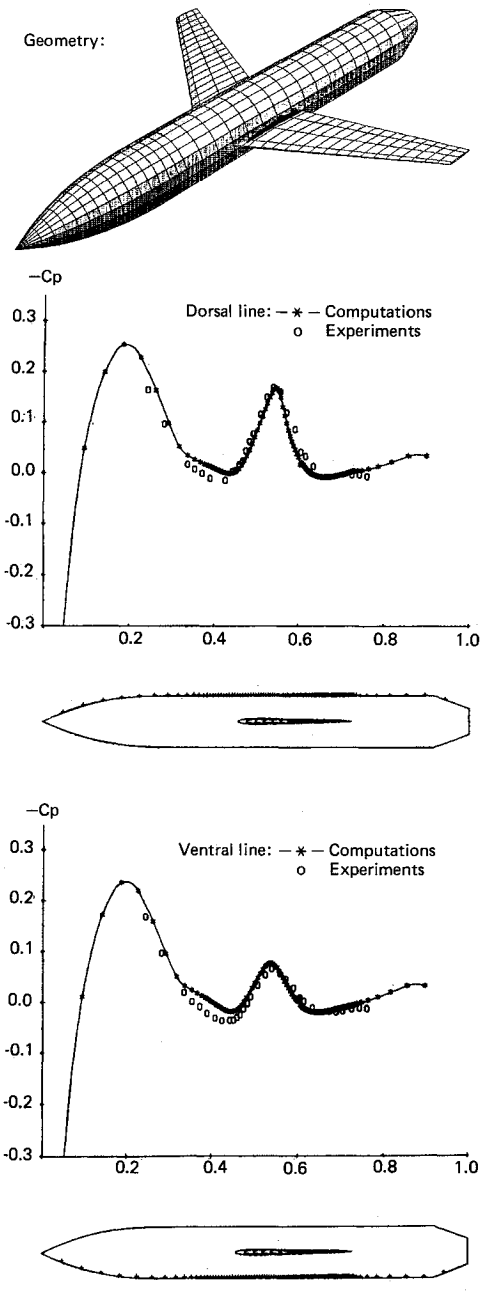

Fig. 7a Computed and experimental[13] pressure signatures for the RAE wing/body at $M_\infty = 0.90$, $\alpha = 1$ deg.

noise, since it has been obtained by digitizing from a drawing. Nevertheless, the body pressure signature characterized by the suction peak over the canopy is in good agreement with wind tunnel data. The wing pressures, including shock positions, are accurately described, except at the leading edge where a finer grid is required.

Finally, note that computed pressure distributions on the body surface are of good quality also for the coarse grids. The fine grids are, however, necessary to produce accurate results on the wing surface. This is particularly so in the leading edge region, where even the finest discretization levels used have been insufficient to catch the suction peak properly. A requirement of, say, 0.1% grid-size relative to the local chord along a swept leading edge will, however, result in a tremendous amount of points if a strictly Cartesian grid is used. Work is now in progress to allow for local grid refinement to overcome this difficulty.

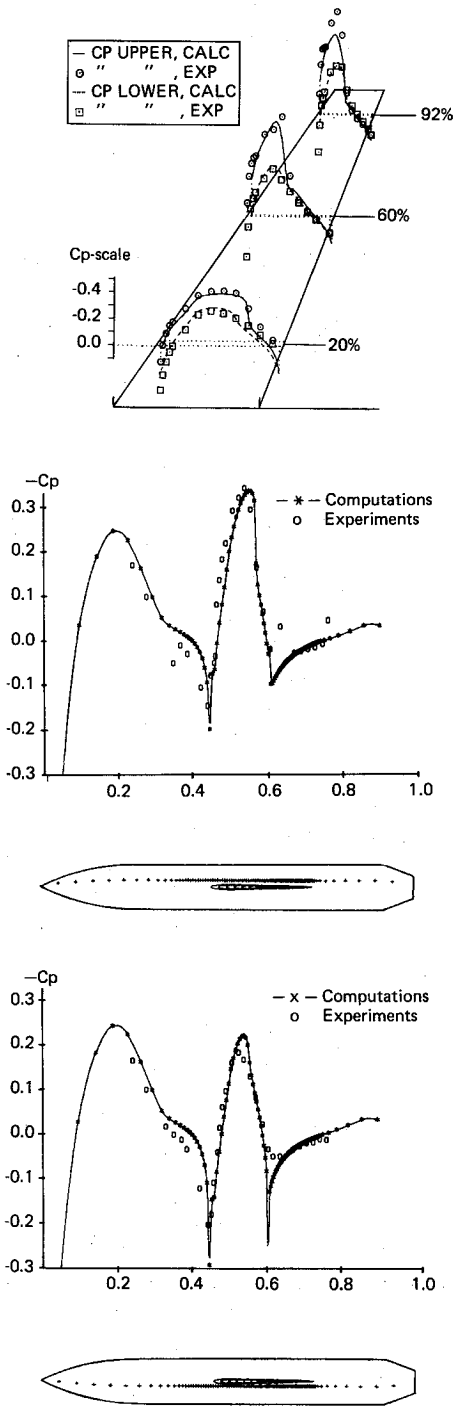

Fig. 7b Wing pressures and body pressures above and below the wing for the RAE wing/body.

Convergence History

A sequence of grids was used for each configuration. The solutions on coarse grids served as initial approximations for the fine grids. The stopping criterion was $c\max < 10^{-4}$, where $c\max$ denotes the maximum potential correction. For the fighter configuration, the convergence was driven further to $c\max < 10^{-5}$, with hardly noticeable changes in the pressure values.

The convergence history for $c\max$ is shown in Fig. 9. When boundary condition updating is activated, as described in Sec. V, we get a temporary increase in $c\max$. During the subsequent iterations, however, $c\max$ decreases rapidly and soon recovers its value prior to the update period.

For the RAE wing-body combination, the average reduction factor for $c\max$ was s and the CPU-time on CRAY-1A was 300 s on the finest grid. The corresponding figures for the fighter configuration were 0.85 and 400 s (to $c\max = 10^{-4}$).

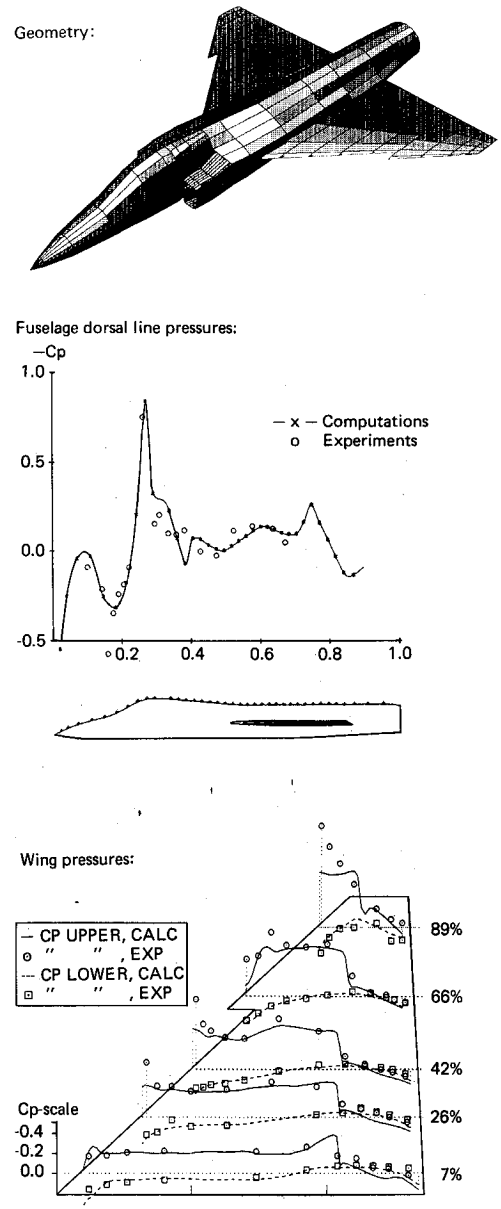

Fig. 8 Computed and experimental pressure signatures for a fighter at $M_\infty = 0.92$, $\alpha = 3.3$ deg.

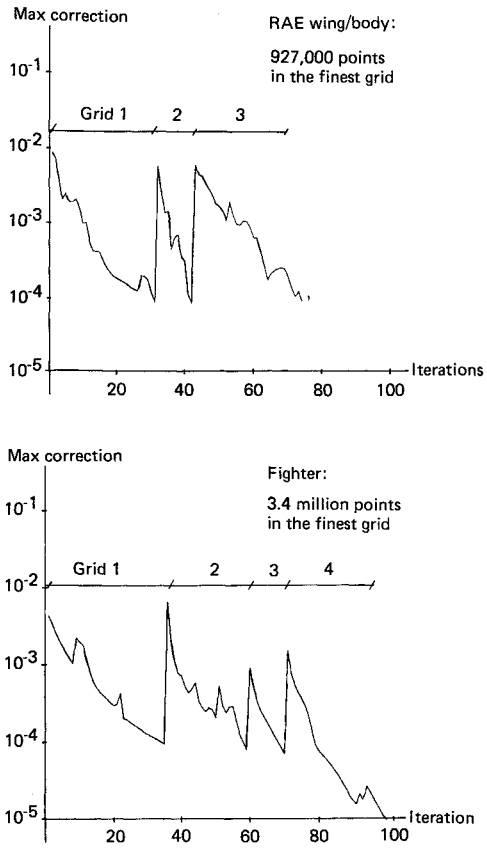

Fig. 9 Convergence history for the RAE wing/body and a fighter configuration.

VII. Conclusions

We have presented a small disturbance formulation for transonic flow computations about wing-fuselage configurations. The concept of the method has been verified and the numerical process is rapidly converging.

Computed pressure distributions on several configurations, including a modern fighter, show good agreement with wind tunnel test data. In particular, wing-body interactions are well-described.

Accurate results in the wing leading edge region require computational grids of high resolution power. Grid point reduction by local grid refinement seems to be an attractive possibility to reduce the computational costs in such cases. So far, encouraging results have been obtained for the ONERA M6 wing, using a hierarchy of embedded, staircase-shaped grids along the leading edge.

References

[1]Akima, H., "A New Method of Interpolation and Smooth Curve Fitting Based on Local Procedures," *Journal of the Association for Computing Machinery* 17(4), Oct. 1970, pp. 589–602.

[2]Ashley, H. and Landahl, M., *Aerodynamics of Wings and Bodies*, Addison-Wesley, 1965.

[3]Bailey, F. R., "On the Computation of Two and Three-Dimensional Steady Transonic Flows by Relaxation Methods," von Kármán Institute Lecture Series: "Progress in Numerical Fluid Dynamics," Feb. 1974.

[4]Boppe, C. W., "Transonic Flowfield Analysis for Wing-Fuslage Configurations," NASA CR-3243, May 1980.

[5]Caap, P. and Elmeland, L., "Calculations of Static Elastic Effects on a Modern High Performance Aircraft," AIAA Paper 86-1771-CP, June 1986.

[6]Fujii, K. and Obayashi, S., "Practical Applications of New LU-ADI Scheme for the Three-Dimensional Navier-Stokes Computation of Transonic Viscous Flows," AIAA Paper 86-0513, Jan. 1986.

[7]Jameson, A., "The Evolution of Computational Methods in Aerodynamics," Princeton University, Princeton, NJ, MAE Rept. 1608, May 1983.

[8]Jameson, A. and Schmidt, W., "Some Recent Developments in Numerical Methods for Transonic Flows," *Computer Methods in Applied Mechanics and Engineering*, Vol. 51, Sept. 1985, pp. 467–493.

[9]Klunker, E. R., "Contribution to Methods for Calculating the Flow about Thin Lifting Wings at Transonic Speeds. Analytical Expressions for the Far Field," NASA TN D-6530, Nov. 1971.

[10]Liepmann, H. W. and Roshko, A., *Elements of Gas Dynamics*, Wiley, New York, 1957.

[11]Murman, E. M., "Analysis of Embedded Shock Waves Calculated by Relaxation Methods," *AIAA Journal*, Vol. 12, May 1974, pp. 626–633.

[12]Taylor, R. A., "Pressure Distributions at Transonic Speeds for Bumpy and Indented Midsections of a Basic Parabolic-Arc Body," NASA Memo 1-22-59A, Feb. 1959.

[13]Treadgold, D. A., Jones, A. F., and Wilson, K. H., "Pressure Distribution Measured in the RAE 8 ft × 6 ft Transonic Wind Tunnel on RAE Wing 'A' in Combination with an Axisymmetric Body at Mach Numbers of 0.4, 0.8, and 0.9," AGARD Advisory Rept. 138, 1979, pp. B4:1–25.

[14]Verhoff, A. and O'Neil, P. J., "Extension of FLO Codes to Transonic Flow Prediction for Fighter Configurations," *Transonic Aerodynamics*, edited by D. Nixon, AIAA, New York, 1982, pp. 467–487.

[15]Woodward, F. A., Analysis and Design of Wing-Body Combinations at Subsonic and Supersonic Speeds, *Journal of Aircraft*, Vol. 5, June 1968, pp. 528–534.